Electronic supporting information:

Gelation enabled charge separation following visible light excitation using self-assembled perylene bisimides

Charlotte L. Smith,[1] Laura L. E. Mears,[1†] Benjamin J. Greeves,[1] Emily R. Draper,[2] James Doutch,[3] Dave J. Adams,[2*] Alexander J. Cowan[1*]

[1] Stephenson Institute for Renewable Energy and the Department of Chemistry, University of Liverpool, Liverpool, L69 7ZF, UK

[2] School of Chemistry, College of Science and Engineering, University of Glasgow, Glasgow, G12 8QQ, UK

[3] STFC ISIS Neutron and Muon Source, Science and Technology Facilities Council, Rutherford Appleton Laboratory, Harwell Oxford, Didcot, OX11 0QX, United Kingdom

[†] Present address, Institute of Applied Physics, Vienna University of Technology, Vienna, 1040, Austria

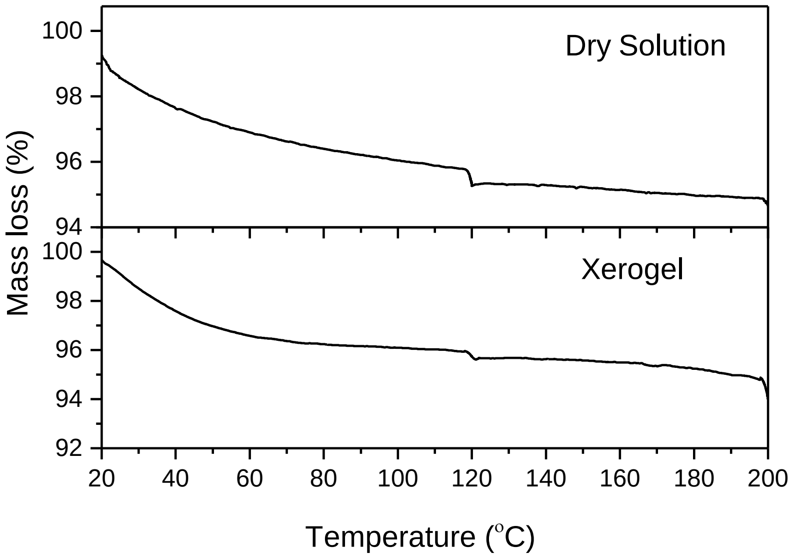

Figure S1: TGA measurements of the dried solutions, xerogel, samples were held for 20 minutes at 120 °C.

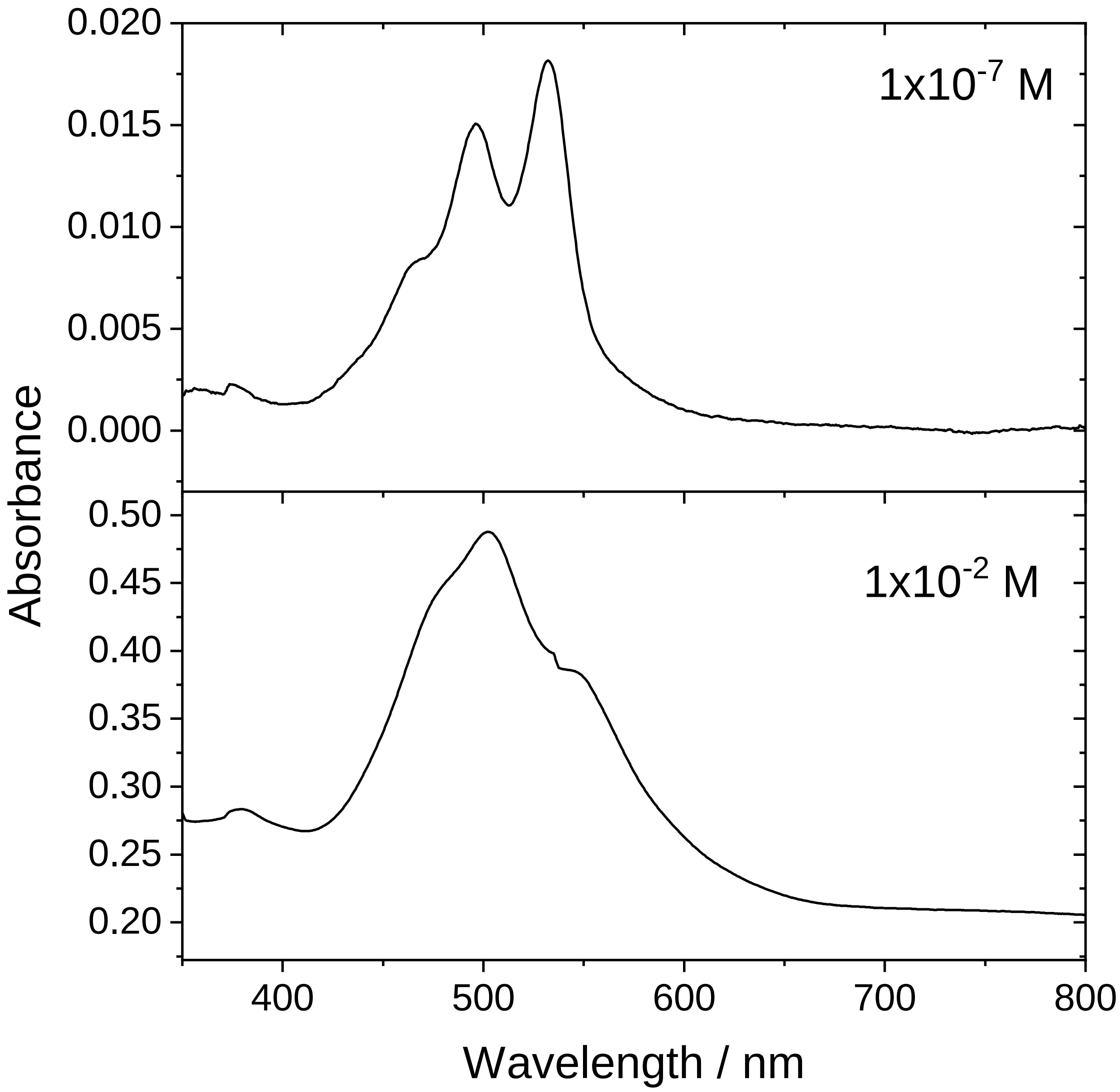

Figure S2: UV/Vis spectra of PBI-A at 1x10^{-7} and 0.01 M in aqueous solution, showing the broadening of features at high concentrations due to the formation of aggregates. The pathlength for the 1 x 10^{-7} M solution is 1 cm. The 0.01 M solution is very strongly absorbing and was recorded by forming a thin layer between two glass slides pressed together.

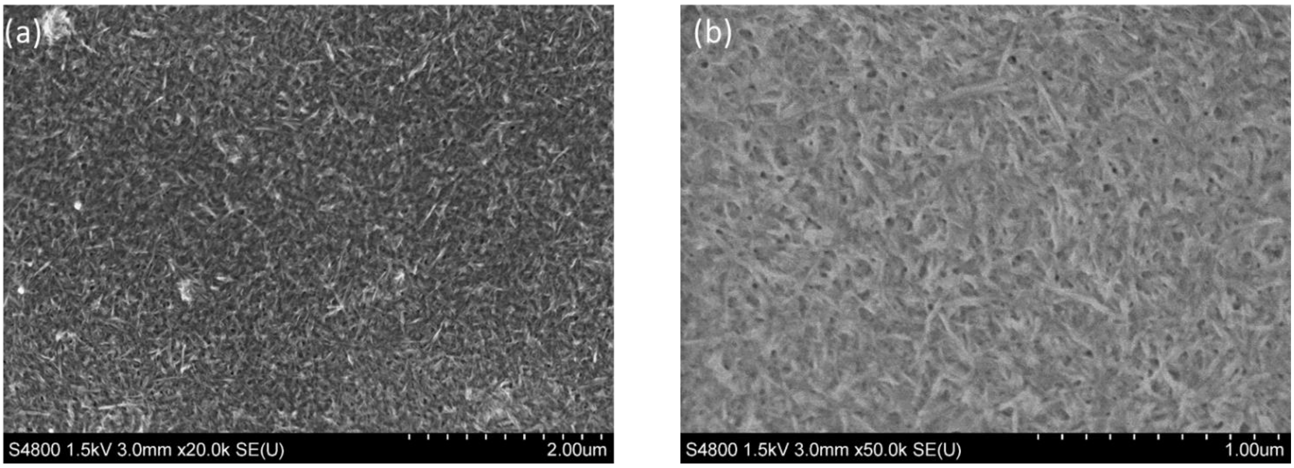

Figure S3: SEM images of a PBI-A xerogel with a 2 µm (a) and 1 µm (b) scale bars, showing fibre bundles. SEM images of PBI-A dried solutions have been reported elsewhere [1].

SANS Fitting

To fit the data for the hydrogel, two models were found to fit well. First, a custom flexible cylinder combined with a power law model within the SASView package was used.[2] The flexible cylinder model assumes a chain with a fixed radius and a contour length, which can be described as a number of locally stiff segments with a length l_p (the Kuhn length is $2xl_p$). A full discussion of the model can be found in the help file of the SASView package.[2,3] To fit the data, the following scattering length densities were used:

D_2O: $6.393x10^{-6}$ Å^{-2}

PBI-A: $3.445x10^{-6}$ Å^{-2}

Air: 0 $x10^{-6}$ Å^{-2}

The parameters extracted from the fit are shown in Table S1. The fit to the combined model as well as the contribution of the two components of the model are shown in Figure S4. Alternatively, a flexible elliptical cylinder model was also found to be as effective (Figure 2). The parameters extracted from the fits shown in Figure 2 are shown in Table S2.

For the xerogel, both models were again found to give good fits to the data. The power law combined with the flexible cylinder (Figure 2, S5) gave a better fit at low Q by eye, as well as a slightly lower chi squared value as compared to the flexible elliptical cylinder model, which also required a very long length to fit (Figure 2).

For the rehydrated xerogel, again both models can be used, with the flexible elliptical cylinder giving a slightly lower value of chi squared. The fit to the combined model as well as the contribution of the two components of the model are shown in Figure S6. The fit to the flexible elliptical cylinder is shown in Figure 2.

In summary, for both models, the SANS data demonstrated that anisotropic aggregated structures were broadly retained in all samples. Using the flexible cylinder combined with a power law implies that drying of the hydrogel to form the xerogel did change the primary fibre dimensions with the radius of fibres decreasing from 5.9 ± 0.2 nm to 3.1 ± 0.3 nm. Rehydration of the xerogel also led to partial, but not complete, recovery of the fibre radius (5.0 ± 0.5 nm). In all cases, the power law needed was similar at 2.4 ± 0.2, 2.6 ± 0.2, and 2.4 ± 0.2 for the hydrogel, xerogel and rehydrated xerogel respectively. By capturing the mass fractal behaviour of the network, the power law changes how the contour length should be interpreted. Therefore, with the combined model it is likely that the model lengths (contour and Kuhn) reflect the complexity of the structures and the distance between entanglements changing and flexible segments within the primary fibres rather as opposed to absolute overall lengths. Hence, whilst there were also changes in the contour length and in the Kuhn length, it is difficult to directly correlate these values, to the microscopy, which clearly shows longer structures, Figure S3, which could be beyond the length scale measurable with SANS. This has also been discussed in detail elsewhere.[4] Note that the scattering from the dried solution is very low, which can be ascribed to a lack of contrast, and hence meaningful fitting of the data was not possible, Figure S7. The data for the hydrogel, xerogel and rehydrated xerogel can also be fitted, essentially equally well, using the flexible elliptical cylinder model, which implies comparatively little change in radius or axis ratio across the samples, with the radius being 2.5 ± 0.1, 3.1 ± 0.3 and 3.0 ± 0.03 nm respectively and the axis ratio being 2.7, 2.7 and 2.8 respectively. For this model, the lengths are all very long. Irrespective of the model used, the radii in all cases are greater than the molecular size and so SANS can be used to show the presence of structures persisting across the hydrogel, xerogel and re-hydrated xerogel state.

Table S1: SANS fitting parameters for the hydrogel, xerogel and rehydrated xerogel spectra using a flexible cylinder model combined with a power law.

	Hydrogel	Xerogel	Rehydrated Xerogel
Power law scale (/10^{-5})	5.7± 0.3	4.3 ± 0.7	3.7 ± 0.2
Power law value, D	2.4 ± 0.02	2.3 ± 0.03	2.5 ± 0.01
Cylinder scale (/10^{-4})	7.4 ± 0.2	2.1 ± 0.03	8.6 ± 0.03
Radius, R (nm)	5.7 ± 0.1	3.5 ± 0.3	5.0 ± 0.7
Kuhn length (nm)	14.3 ± 5.0	7.6 ± 2.2	12.9 ± 1.3
Contour length, L (nm)	56.9 ± 3.0	30.4 ± 7.0	51.2 ± 3.0
Background (cm^{-1})	0.0346 ± 0.001	0.0050 ± 0.0004	0.0022 ± 0.0003

χ^2	3.4	1.6	3.2

Table S2: SANS fitting parameters for the hydrogel, xerogel and rehydrated xerogel spectra using a flexible elliptical cylinder model.

	Hydrogel	Xerogel	Rehydrated Xerogel
Cylinder scale (/10^{-4})	7.8 ± 0.1	2.8 ± 0.01	0.5 ± 0.01
Radius, R (nm)	2.5 ± 0.1	3.1 ± 0.3	3.0 ± 0.03
Axis ratio	2.7 ± 0.1	2.7 ± 0.08	2.8 ± 0.06
Kuhn length (nm)	6.3 ± 0.1	5.8 ± 0.1	23.4 ± 1.4
Contour length, L (nm)	>1000	>1000	496 ± 120
Background (cm^{-1})	0.0387 ± 0.01	0.0064 ± 0.001	0.0038 ± 0.0002
χ^2	3.1	2.2	2.4

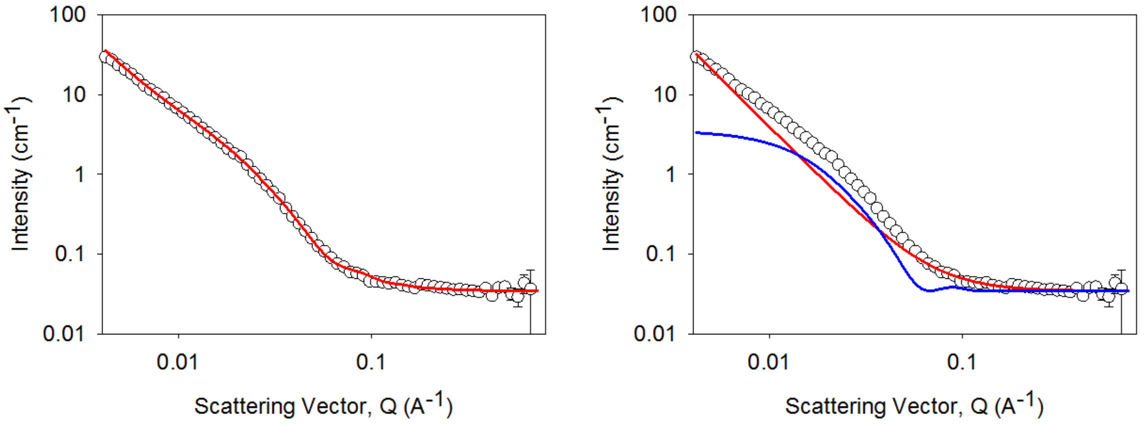

Figure S4: SANS of a hydrogel of 1.0 mm thickness. (Left) A custom flexible cylinder combined with a power law model within SasView package was used, and parameters are given in Table S1. The fit for the data is given as a red solid line. (Right) The relative contribution of the power law (red) and flexible cylinder (blue) model to the combined model is shown.

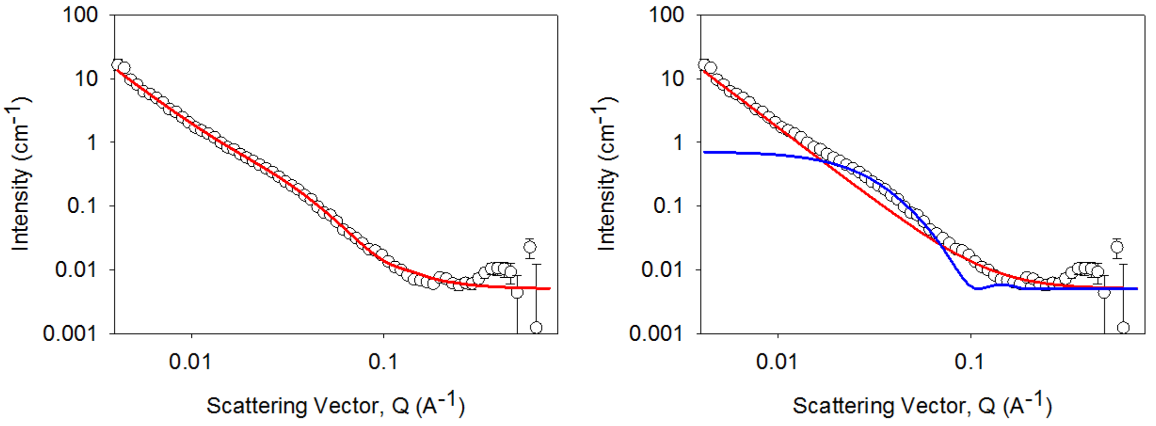

Figure S5: SANS of a xerogel prepared from a 1.0 mm thick hydrogel. A custom flexible cylinder combined with a power law model within SasView package was used, and parameters are given in Table S1. The fit for the data is given as a red solid line. (Right) The relative contribution of the power law (red) and flexible cylinder (blue) model to the combined model is shown.

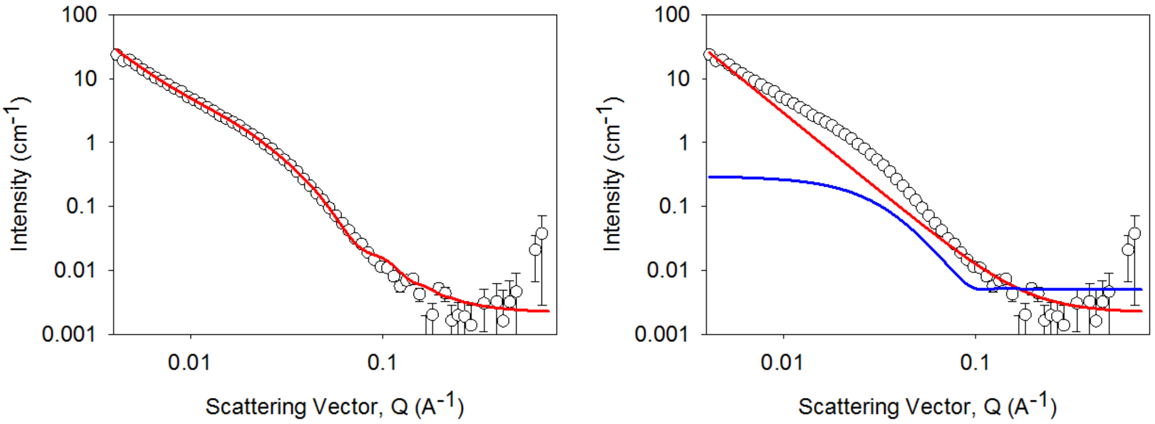

Figure S6: SANS of rehydrated xerogel after rehydration in 0.1 M KCl electrolyte, pD4, in D_2O for 50 hours. The remainder of the 1 mm demountable cell thickness was filled with 0.1 M KCl electrolyte, pD 4, in D_2O. A custom flexible cylinder combined with a power law model within SasView package was used, and parameters are given in Table S1. The fit for the data is given as a red solid line. (Right) The relative contribution of the power law (red) and flexible cylinder (blue) model to the combined model is shown.

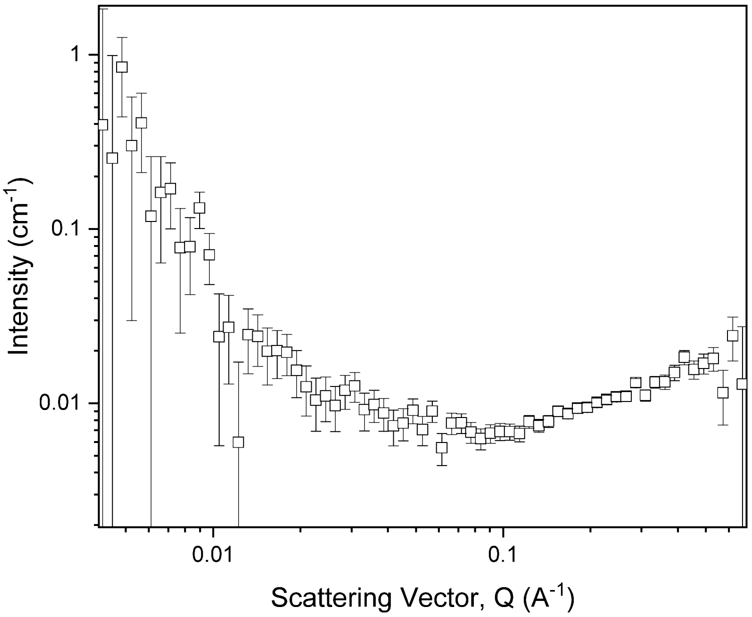

Figure S7: SANS of a dried solution of PBI-A. The same volume as used for the gel samples was dried on a quartz disc and the sample received the same exposure to the neutron beam as all the gels. Note that the scattering intensity is very low, the improvement of the error bars would require a significantly longer (eg 16 times) exposure, which can be ascribed to a lack of contrast.

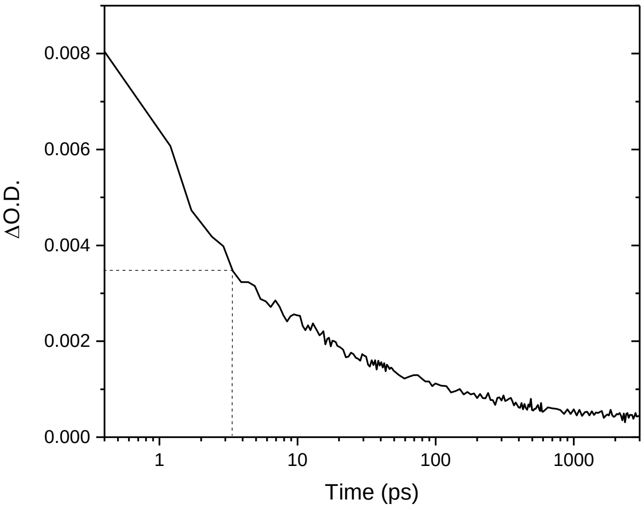

Figure S8: Decay of 740 nm TA feature following visible excitation of a PBI-A dried solution (490 nm, 275 µW, 5 kHz excitation repetition rate). The dashed line shows the time taken for the change in optical density to decrease by 50% compared to its greatest value.

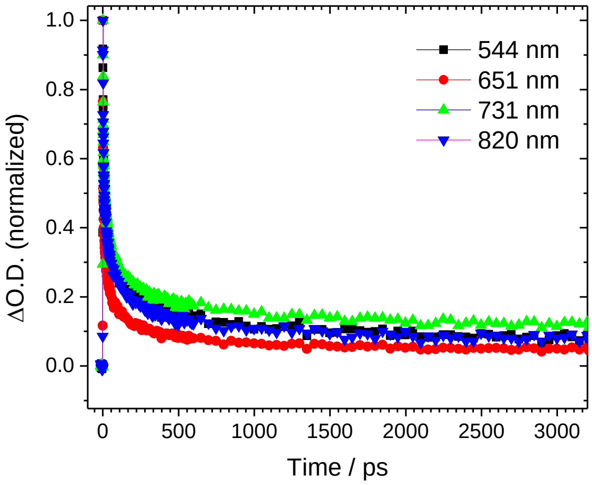

Figure S9: Single wavelength kinetics following visible excitation of a PBI-A hydrogel (490 nm, 275 µW, 5 kHz excitation repetition rate).

LDA fitting: LDA fitting was carried out using the Optimus[5] software package. Prior to analysis all data was manually chirp corrected for velocity dispersion. Initially the instrument response function was fitted (0.3 ps) and held constant throughout the LDA fitting process. A minimum of 50 regularization factors (spanning 0.01 to 5) were used. For the rehydrated xerogel 100 factors were required to find the point of greatest curvature in the L-curve. Fitting was completed using 100 exponential lifetimes distributed over a 5000 ps timescale.

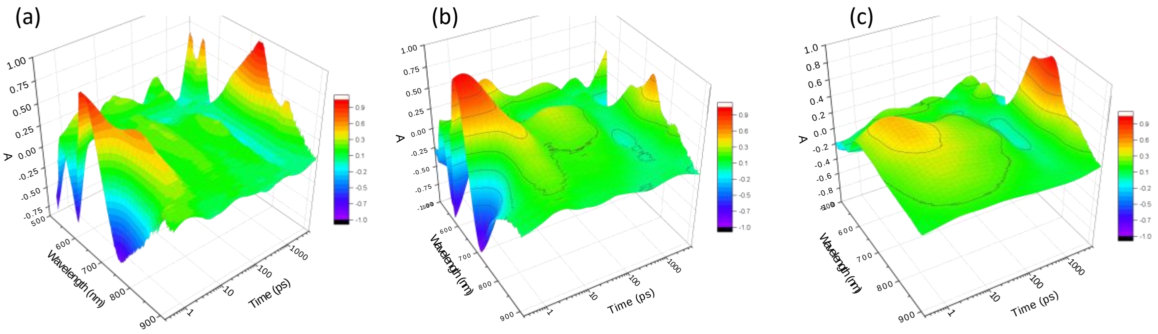

Figure S10. *3D plots of the lifetime distribution maps (LDM) for PBI-A hydrogel (a), rehydrated xerogel (b) and xerogel (c) following visible light excitation (490 nm).*

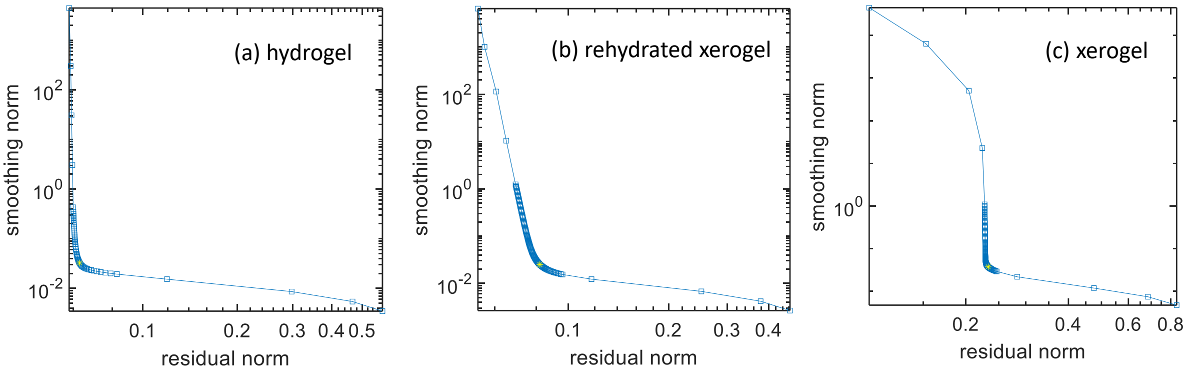

Figure S11: L-curves generated within the Optimus[5] programme during LDA. LDM shown within the main text are generated with a regularization factor identified (shown as a yellow cross) through visual analysis of the L-curve.

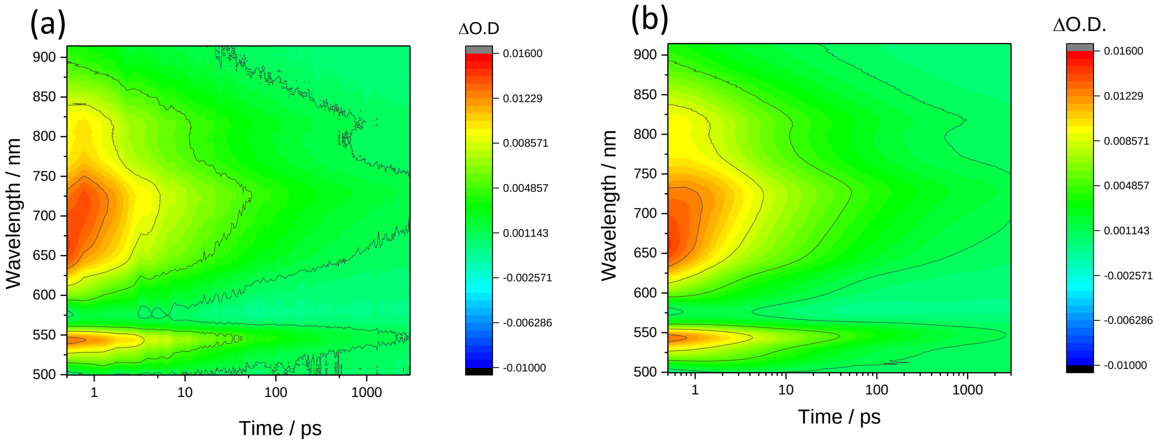

Figure S12: (a) Raw TA data (chirp corrected) compared to (b) reconstructed data based on LDA output presented in the main text for the visible light excitation of a hydrogel sample

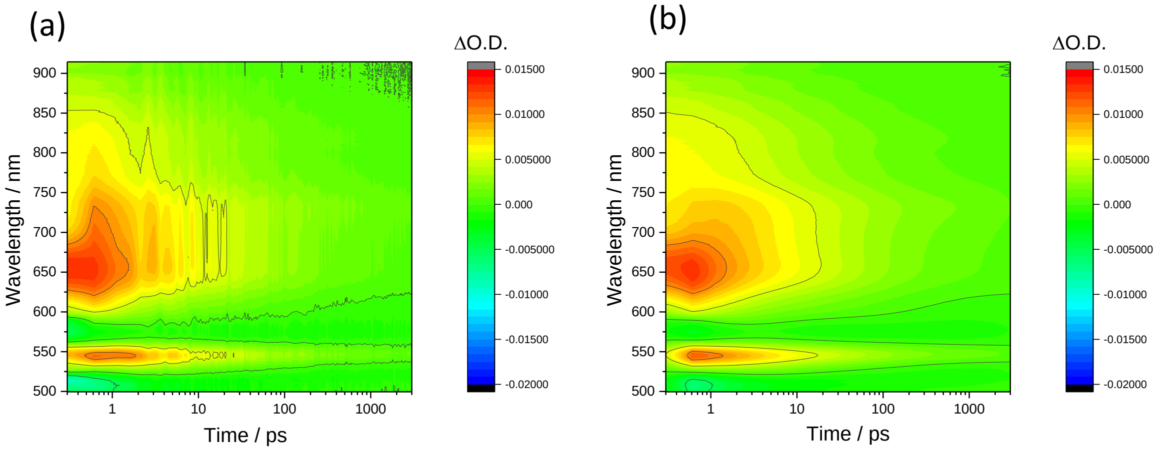

Figure S13: (a) Raw TA data (chirp corrected) compared to (b) reconstructed data based on LDA output presented in the main text for the visible light excitation of a rehydrated xerogel sample.

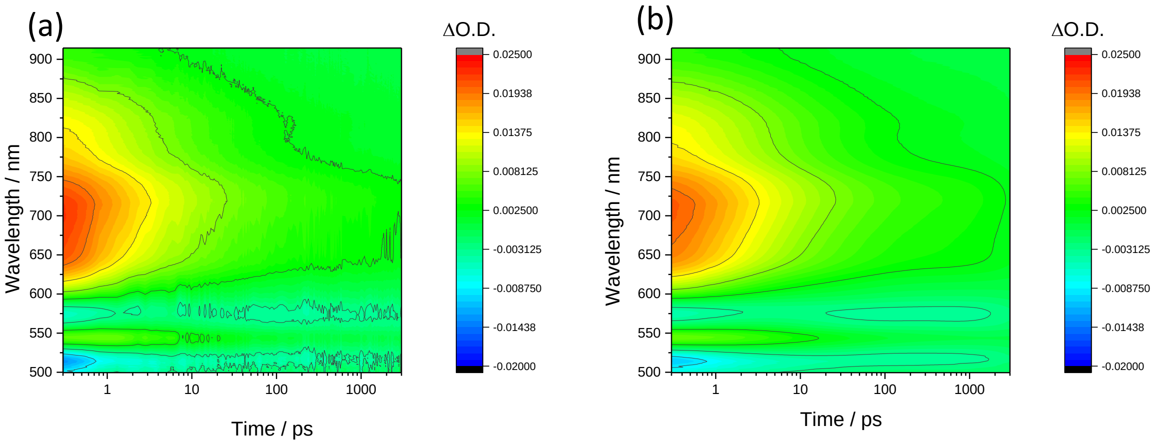

Figure S14: (a) Raw TA data (chirp corrected) compared to (b) reconstructed data based on LDA output presented in the main text for the visible light excitation of a xerogel sample

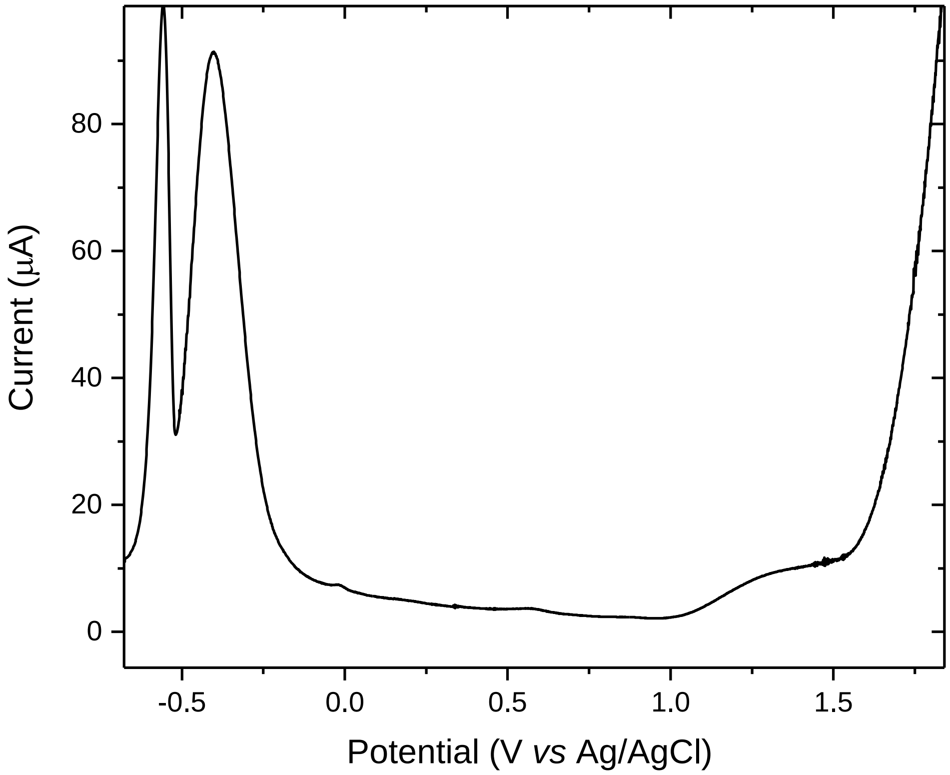

Figure S15: Square wave voltammogram of a PBI-A hydrogel under a nitrogen atmosphere, scanning from -0.75 V to + 1.8 V at a frequency of 25 Hz with an equilibration time of 120 seconds. The feature at -0.40 $V_{Ag/Agcl}$ is assigned to PBI-A/PBI$^{\bullet-}$-A and the reduction at -0.60 $V_{Ag/Agcl}$ is assigned to PBI$^{\bullet-}$-A / PBI^{2-}. The assignment of the band at 1.25 V is described in detail in the main text.

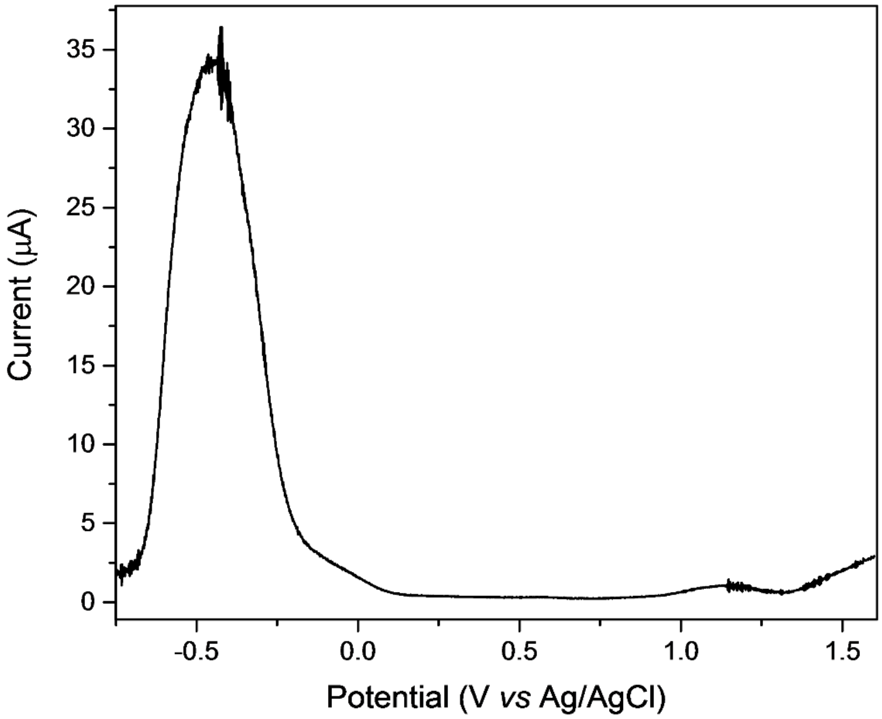

Figure S16: Square wave voltammogram of a PBI-A rehydrated xerogel under a nitrogen atmosphere, scanning from -0.75 V to +1.55 V at a frequency of 25 Hz with an equilibration time of 90 seconds. The broad feature between -0.2 to -0.6 V is assigned to a combination of PBI-A/$PBI^{\bullet -}$-A and $PBI^{\bullet -}$-A / PBI^{2-}, DCVA (see figure S20) is used below to separately identify these two close lying reductions. The assignment of the band at 1.15 V is described in detail in the main text.

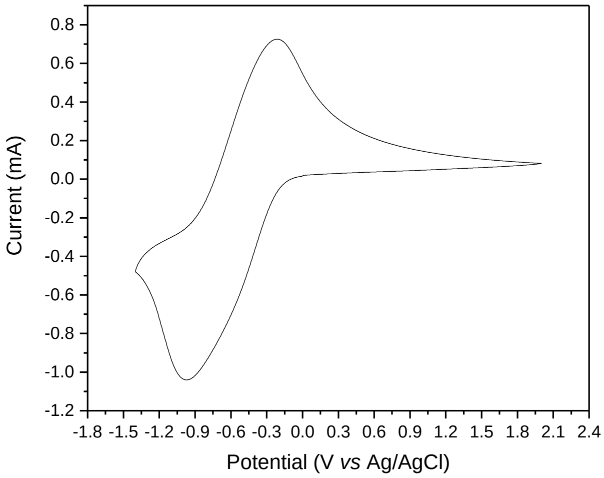

Figure S17: Cyclic voltammogram in 0.1 M KCl (pH 4) of a hydrogel PBI-A sample at 100 mV s^{-1}.

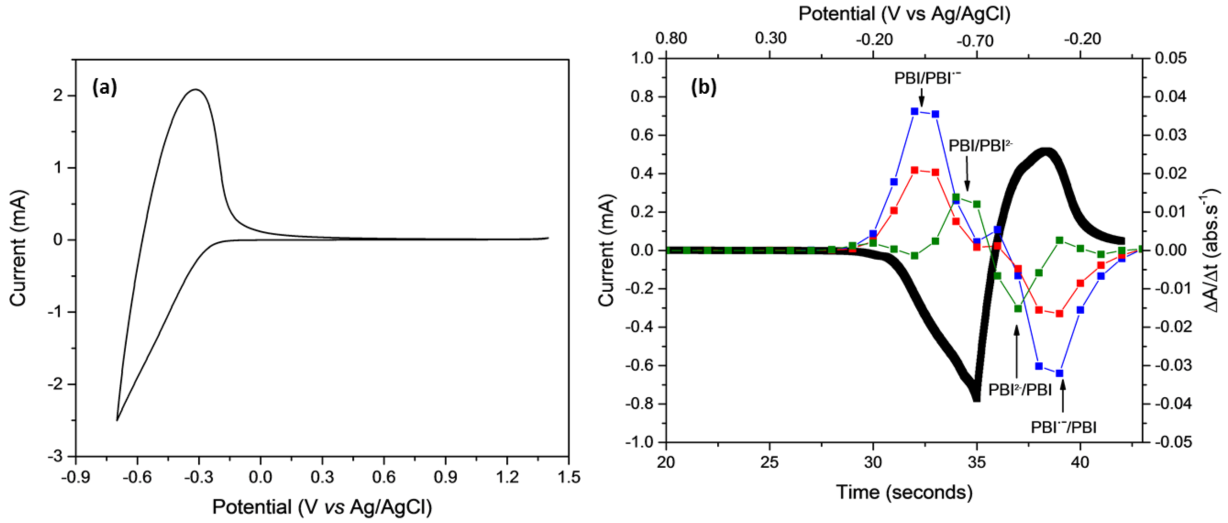

Figure S18: Xerogel CV in 0.1 M KCl (pH 4) under an atmosphere of argon at 100 mVs^{-1} (a) DCVA data of a rehydrated xerogel (b) shows the formation of PBI$^{\bullet-}$-A and PBI^{2-}-A upon reduction on FTO glass during a CV (black) allowing for the assignment of electrochemical reduction features. Differential absorbance at 729 nm (blue trace, PBI$^{\bullet-}$-A), 820 nm (red trace, PBI$^{\bullet-}$-A) and 608 nm (green trace, PBI^{2-}-A) are shown.

DCVA measurements: The CV and square wave voltammogram of the xerogel sample does not show well-defined reduction features for these processes. Using differential cyclic voltabsorptometry (DCVA), it is possible to accurately measure the reduction potentials of close lying electrochemical states.[6] In a DCVA measurement, the rate of change in absorbance at a particular wavelength is plotted against the potential during the CV measurement. Electrochemically-generated species appear as positive features with maxima at the potential where the maximum current for the same electrochemical process would be measured in the CV. The optical response is free of background capacitance, and providing minimal spectral overlap between species, it appears as a well-defined maximum. In Figure 3c, the DCVA spectra of a rehydrated PBI-A xerogel recorded at wavelengths corresponding to PBI$^{\bullet-}$-A (730 nm and 820 nm) and PBI^{2-}-A (608 nm) are shown. From these data, the reduction potentials for PBI$^{0/-}$-A and PBI$^{\bullet-/2-}$-A of -0.46 V and -0.66 V are obtained.

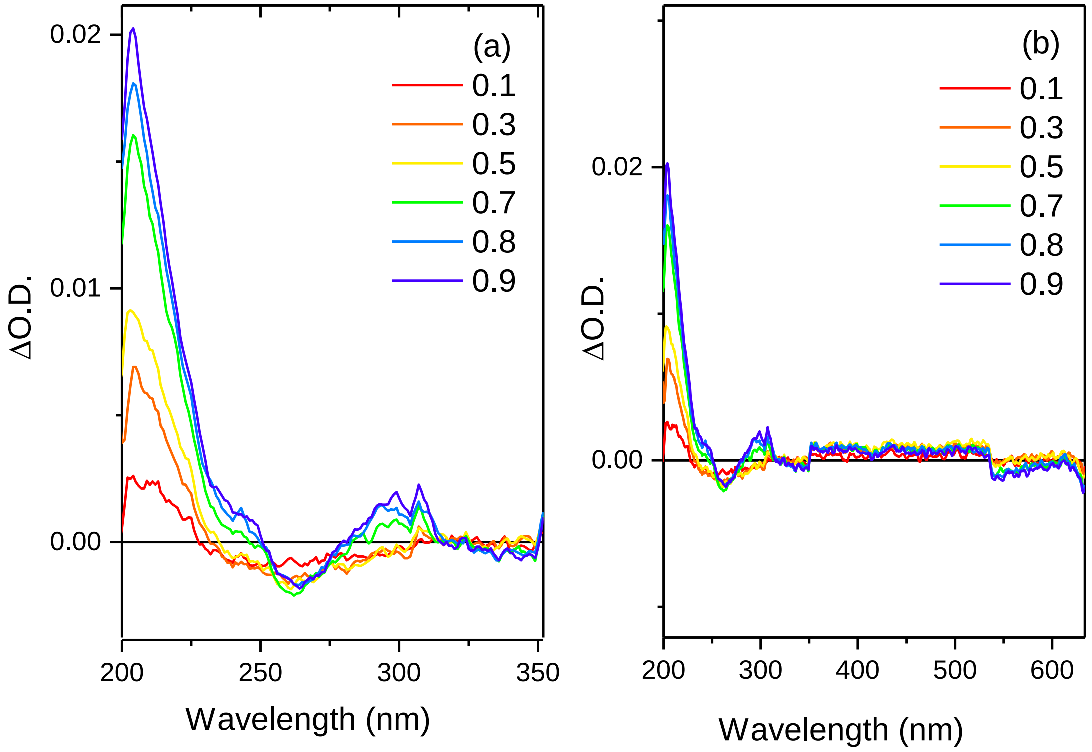

Figure S19: Spectroelectrochemistry of the PBI-A rehydrated xerogel oxidation. Experiments are carried out at pH 4, 0.1 M KCl. Spectra are shown with an expansion of the region showing the greatest changes (a) and the wider PBI S_0-S_1 transition (b). Voltages are versus a silver pseudo reference electrode.

Table S3: Calculated Gibbs energy of photoinduced electron transfer from the intramolecular alanine donor functionality to the PBI core.

	$E_{OX\ ALANINE}$ ($V_{Ag/AgCl}$)	$E_{RED\ PBI}$ ($V_{Ag/AgCl}$)	E^* (eV)	C (eV)	S (eV)	ΔG_{ET} (eV)
Rehydrated xerogel	1.15	-0.46	2.13	0.03	0	-0.55
Hydrogel	1.25	-0.40	2.17	0.03	0	-0.55
Xerogel	1.15	-0.46	2.13	0.68	1.26	0.06

$$\Delta G_{ET} = E_{OX} - E_{RED} - E^* - \frac{e^2}{4\pi r_{DA}\varepsilon_0\varepsilon_s} + \frac{e^2}{8\pi\varepsilon_0}\left(\frac{1}{r_D} + \frac{1}{r_A}\right)\left(\frac{1}{\varepsilon_s} - \frac{1}{\varepsilon_p}\right) \quad \text{Eq. S1}$$

$$\Delta G_{ET} = E_{OX} - E_{RED} - E^* - C + S \quad \text{Eq. S2}$$

Table S3. is derived using Equation S1, 2 and the electrochemical data described in the main paper. In Equation 1 E_{ox} (alanine) is measured by square wave voltammetry (see Figure S13,14), E_{red} (PBI) is measured either by square wave voltammetry (hydrogel) or DCVA (rehydrated xerogel). For the hydrogel and rehydrated xerogel the electrochemical data is recorded in the same electrolyte as is used in the photoelectrochemical and transient studies, therefore there is no difference in solvation energy between the photogenerated charge separated state and the electrochemically oxidised and reduced species ($\varepsilon_s = \varepsilon_p$), making the solvation term (*S*) in Equation S2 zero. For the (dry) xerogel the electrochemical data for the rehydrated xerogel was used and the *S* term was calculated using a local dielectric of ~3 for the dried PBI-A xerogel and ~80 for the aqueous electrochemistry. The ionic radii for the donor and acceptor groups was taken from a past study on PBI-A.[1] E* is calculated from the average of the energies of its 0-0′ absorption maximum and emission maximum. The Coulombic interactions (*C*) between the two ions is calculated as shown in Equation S1 where the donor-acceptor distance (r_{DA}) is taken to be the distance between the chiral carbon atom of the amino acid and centre of the PBI core, *ca.* 7 Å as calculated in a previous study.[1]

References

1. Walsh, J. J. *et al.* Controlling Visible Light Driven Photoconductivity in Self-Assembled Perylene Bisimide Structures. *J. Phys. Chem. C* **120**, 18479–18486 (2016).
2. www.sasview.org.
3. Draper, E. R. *et al.* Using the hydrolysis of anhydrides to control gel properties and homogeneity in pH-triggered gelation. *RSC Adv.* **5**, 95369–95378 (2015).
4. Mears, L. L. E. *et al.* Drying Affects the Fiber Network in Low Molecular Weight Hydrogels. *Biomacromolecules* **18**, 3531–3540 (2017).
5. Slavov, C., Hartmann, H. & Wachtveitl, J. Implementation and Evaluation of Data Analysis Strategies for Time-Resolved Optical Spectroscopy. *Anal. Chem.* **87**, 2328–2336 (2015).
6. Walsh, J. J. *et al.* Directing the mechanism of CO 2 reduction by a Mn catalyst through surface immobilization. *Phys. Chem. Chem. Phys.* **20**, 6811–6816 (2018).